THE JOURNAL OF PHYSICAL CHEMISTRY Letters

Letter

pubs.acs.org/JPCL

Photoferroelectric and Photopiezoelectric Properties of Organometal Halide Perovskites

Shi Liu,*[,†] Fan Zheng,[‡] Ilya Grinberg,[‡] and Andrew M. Rappe*[,‡]

[†]Geophysical Laboratory, Carnegie Institution for Science, Washington, DC 20015-1305, United States

[‡]The Makineni Theoretical Laboratories, Department of Chemistry, University of Pennsylvania, Philadelphia, Pennsylvania 19104−6323, United States

ABSTRACT: Piezoelectrics play a critical role in various applications. The permanent dipole associated with the molecular cations in organometal halide perovskites (OMHPs) may lead to spontaneous polarization and thus piezoelectricity. Here we explore the piezoelectric properties of OMHPs with density functional theory. We find that the piezoelectric coefficient depends sensitively on the molecular ordering and that the experimentally observed light-enhanced piezoelectricity is likely due to a nonpolar to polar structural transition. By comparing OMHPs with different atomic substitutions in the ABX_3 architecture, we find that the displacement of the *B*-site cation contributes to nearly all of the piezoelectric response and that the competition between *A*−*X* hydrogen bond and *B*−*X* metal−halide bond in OMHPs controls the piezoelectric properties. These results highlight the potential of the OMHP architecture for designing new functional photoferroelectrics and photopiezoelectrics.

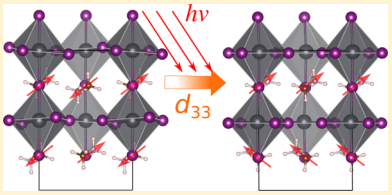

Organometal halide perovskites (OMHPs) with their unprecedented rate of increasing power conversion efficiency (PCE)[1] have transformed photovoltaic (PV) research and development. These materials, especially methylammonium lead iodide ($MAPbI_3$), are promising candidates for next-generation low-cost-to-power PV technologies.[2−8] Besides the solar cell application, the OMHP architecture, consisting of ABX_3 (organic monovalent cation, *A*; divalent metal, *B*; inorganic or organic anion, *X*), could serve as a promising platform for the design and optimization of materials with desired functionalities. By substituting ABX_3 atomic constituents, it is feasible to controllably tune the structural, electronic, optical, and magnetic properties of functional materials.[9]

Piezoelectrics (materials that can convert between electrical and mechanical energy) are a class of technologically important materials with a variety of applications, ranging from waveguide devices, ultrasound transducers, and fuel injectors to accelerometers and gyroscopes.[10,11] The permanent dipole provided by the organic molecule in OMHPs is suggested to give rise to spontaneous polarization, which may play an important role in the PV working mechanism.[12−14] Switchable polar domains in β-$MAPbI_3$ have been observed via piezoresponse force microscopy (PFM).[15] Although the robustness of the room-temperature ferroelectricity in $MAPbI_3$ is still under debate,[16−19] the piezoelectric response of $MAPbI_3$ has been demonstrated experimentally via PFM.[19] In particular, a 5-fold increase in piezoelectric coefficient under illumination was observed.[19] Furthermore, the piezoelectric coefficient of $MAPbI_3$ under light (∼25 pm/V) is comparable to inorganic ferroelectric thin films, such as lead zirconate titanate (PZT) thin films.[20] The optically tunable high piezoelectric response in $MAPbI_3$ suggests potential applications of OMHPs for optical piezoelectric transducers and light-driven electromechanical transistors.

In this work, we investigate the piezoelectric properties of OMHPs with density functional theory (DFT). The interplay between the *A*-site molecular ordering and the macroscopic piezoelectric response is explored by quantifying the polarization-strain ($P-\eta$) and polarization-stress ($P-\sigma$) relationships in two model structures with designed molecular orientations. We further study the effect of atomic substitution with different organic molecules at the *A* site ($CH_3NH_3^+$, $CF_3NH_3^+$), metal cations at the *B* site (Pb^{2+}, Sn^{2+}, Ge^{2+}), and halide anions at the *X* site (I^-, Cl^-). Our calculations show that the competition between the *A*−*X* hydrogen bond and the *B*−*X* metal−halide bond in OMHPs gives rise to a range of piezoelectric properties. The strong dependence of piezoelectric coefficients on the molecular ordering suggests that the light-enhanced piezoelectricity is likely due to the light-induced molecular reorientation under external voltage. This work demonstrates that the OMHP architecture could serve as a promising platform for designing functional piezoelectrics with robust optical tunability.

All calculations are performed with a plane-wave implementation of the Perdew−Burke−Ernzerhof (PBE) density functional[21] in the QUANTUM-ESPRESSO code.[22] The optimized norm-conserving pseudopotentials[23,24] are generated using the OPIUM[23,24] code with the following electronic states included as valence states: Pb: 5d, 6s, 6p; I: 4d, 5s, 5p; C: 2s, 2p; N: 2s, 2p; H: 1s. A 4 × 4 × 4 Monkhorst−Pack grid is used, consistent with our previous work.[13,25] The effect of molecular orientation on piezoelectricity is explored by calculating the piezoelectric coefficients of two model structures, namely, M1

Received: March 6, 2016
Accepted: March 22, 2016
Published: March 22, 2016

DOI: 10.1021/acs.jpclett.6b00527
J. Phys. Chem. Lett. 2016, 7, 1460−1465

with nonzero total polarization and M2 with net-zero polarization, shown in Figure 1. The M1 structure has an

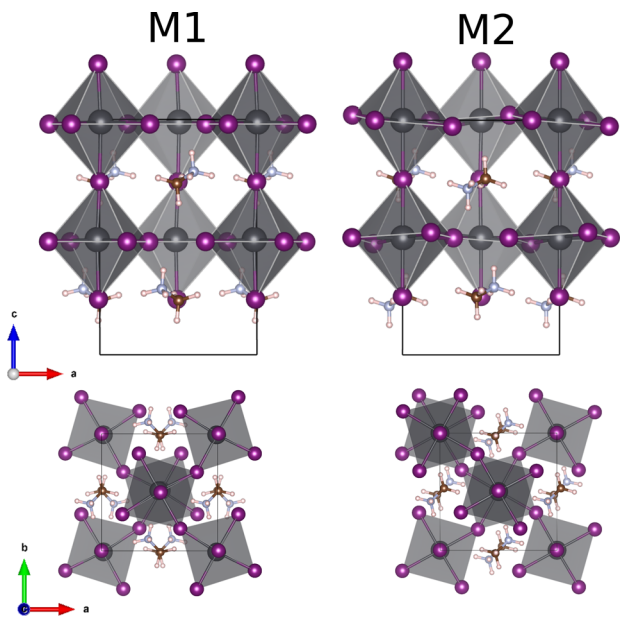

Figure 1. Side view and top view of polar (M1) and nonpolar (M2) structural models for $MAPbI_3$. The M1 configuration has molecular dipoles aligned preferentially along the *c* axis while distributed isotropically within the *ab* plane. The molecules in the M2 configuration adopt an antiferroelectric arrangement.

isotropic orientation of the MA cations in the *ab* plane and an anisotropic orientation with respect to the *c* axis, giving rise to a net polarization along the *c* axis. The molecular dipoles in the M2 structure adopt an antiferroelectric ordering, and the structure is globally (nearly) paraelectric. These two models are representative of possible molecular orientations in OMHPs and have been previously used to reveal the effect of polar order on bulk PV effects[25] and the dynamics of molecular cations.[26]

First-principles techniques to determine piezoelectric coefficients have been widely applied to inorganic materials.[27−30] As piezoelectricity is a fundamental process incorporating different electromechanical effects, multiple piezoelectric equations exist.[11,30,31] The *direct* piezoelectric effect that links the induced polarization that develops in direction i (ΔP_i) with an applied stress with component j (σ_j in Voigt notation) can be described by

$$\Delta P_i = d_{ij}\sigma_j \quad (1)$$

where $\{d_{ij}\}$ is a third-rank tensor and each d_{ij} parameter is usually referred to as a *direct* piezoelectric coefficient or piezoelectric strain coefficient, in units of pC/N. Another piezoelectric equation connecting the strain η and the polarization is given by

$$\Delta P_i = e_{ij}\eta_j \quad (2)$$

where the e_{ij} parameter is called the piezoelectric stress coefficient in the unit of C/m^2. It is noted that the e_{ij} and d_{ij} parameters are related to each other via elastic compliances or stiffness, although d_{ij} is easier to measure experimentally. In this study, we focus on the evaluation of d_{33} and e_{33} (piezoelectric response along the *c* axis). The total induced polarization along the *c* axis can be expressed as $\Delta P_3 = e_{33}\eta_3 + e_{31}(\eta_1+\eta_2)$, where $\eta_1 = (a - a_0)/a_0$, $\eta_2 = (b - b_0)/b_0$, and $\eta_3 = (c - c_0)/c_0$ are strains along the *a*, *b*, and *c* axes, and a_0, b_0, and c_0 are lattice constants of an unstrained structure. When only applying strain along the *c* axis, e_{33} can be evaluated from the slope of polarization versus strain (η_3) curve. For a given strain η_3, the internal atomic coordinates are fully relaxed until the residual forces on atoms are $<1.0 \times 10^{-5}$ Ryd/Bohr, and the polarization of the optimized structure is determined with the Berry's phase approach. The estimation of d_{33} with DFT is less straightforward due to the difficulty of defining the stress tensor. We adopt the finite difference method developed in ref 32. After applying a strain along the [001] direction, the other lattice parameters (lattice constants *a* and *b* and lattice angles) as well as internal atomic coordinates are fully optimized until all stress tensor elements except σ_3 are $<1.0 \times 10^{-3}$ GPa. The polarization values of various strained structures are then calculated, and the slope of *P* versus σ_3 determines the value of d_{33}. For each material investigated, the structure is first fully optimized to obtain the equilibrium lattice constants, and ±0.5% strains are applied to the ground-state structures to obtain linear response.

A previous first-principles benchmark study highlighted the importance of dispersive interactions and the plane-wave cutoff energy (E_c) in accurately determining structural properties of OMHPs.[33] Because the value of piezoelectric coefficient depends sensitively on the lattice constants, we first compare the optimized structural parameters of $MAPbI_3$ obtained with four different methods: pure PBE density functional with E_c = 50 Ry, PBE with E_c = 80 Ry, PBE plus Grimme dispersion correction[34](PBE-D2) with E_c = 50 Ry, and PBE-D2 with E_c = 80 Ry. As shown in Table 1, the value of unit cell volume

Table 1. Structural Parameters of Tetragonal $MAPbI_3$ in the M1 Configuration Compared with Experimental Data

	method	E_c (Ry)	*a* (Å)	*b* (Å)	*c* (Å)	*α*	*β*	*γ*	*V* (Å^3)
M1	PBE	50	8.91	8.81	13.09	90.00	90.00	90.03	1027.10
	PBE	80	8.97	8.92	13.29	90.01	90.03	90.00	1062.87
	PBE-D2	50	8.64	8.68	12.77	90.05	89.86	89.92	957.93
	PBE-D2	80	8.67	8.74	12.97	90.07	89.87	90.00	981.90
M2	PBE	50	8.88	8.89	13.06	91.18	91.39	89.75	1030.33
	PBE	80	8.99	8.96	13.22	91.27	90.04	89.71	1063.54
	PBE-D2	50	8.63	8.64	12.82	90.41	90.45	90.17	955.71
	PBE-D2	80	8.69	8.69	12.97	90.09	90.10	90.06	979.83
	experiment	ref 8	8.85	8.85	12.64	90.0	90.0	90.0	990.00
		ref 42	8.86	8.86	12.66	90.0	90.0	90.0	993.80
		ref 3	8.85	8.85	12.44	90.0	90.0	90.0	974.33

DOI: 10.1021/acs.jpclett.6b00527
J. Phys. Chem. Lett. 2016, 7, 1460−1465

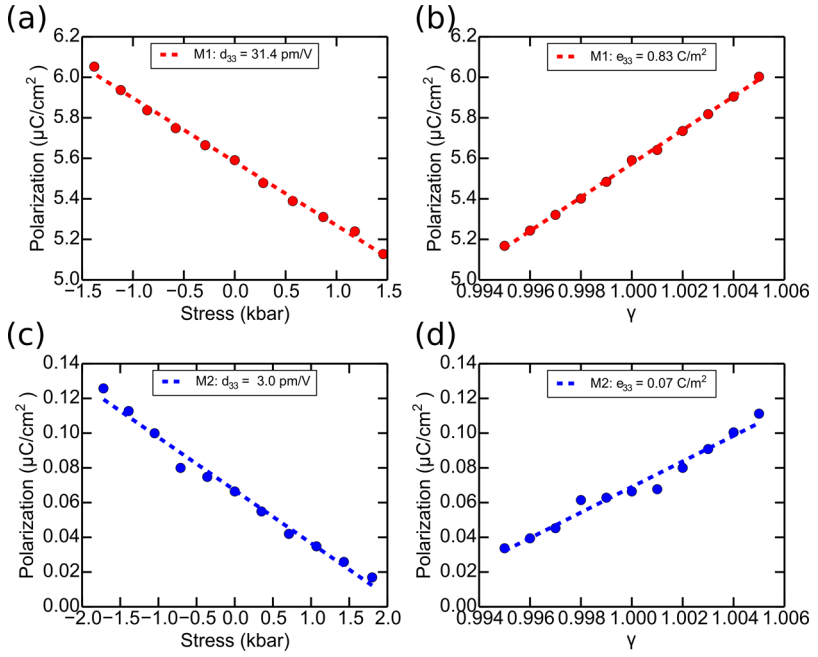

Figure 2. Piezoelectric properties of $MAPbI_3$ in M1 (a,b) and M2 (c,d) configurations. (a,c) Polarization as a function of stress. (b,d) Polarization as a function of strain.

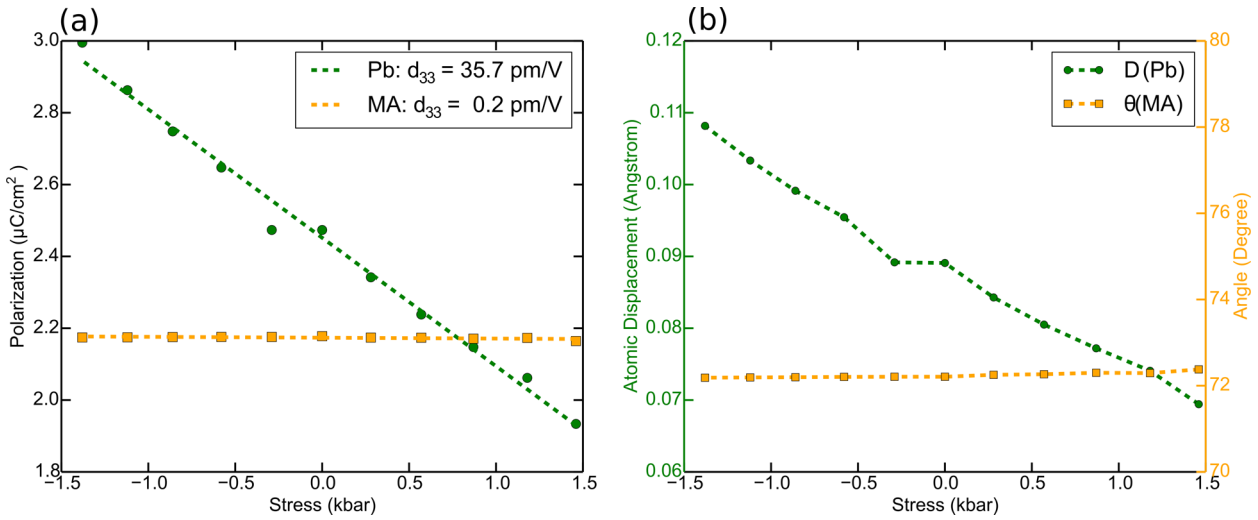

Figure 3. (a) Site-resolved polarization as a function of stress. (b) Atomic displacement and molecular orientational angle as a function of stress.

predicted by PBE-D2 with E_c = 80 Ry best agrees with the experimental results. Therefore, we choose this method for the following piezoelectric coefficient calculations.

Figure 2 shows the $P-\sigma_3$ and $P-\eta_3$ curves for $MAPbI_3$ in polar M1 and nonpolar M2 configurations. The computed piezoelectric coefficients of M1 are d_{33} = 31.4 pm/V and e_{33} = 0.83 C/m^2, dramatically higher than those of M2, d_{33} = 3.1 pm/V and e_{33} = 0.07 C/m^2. Note that the values of d_{33} of M1 and M2 agree reasonably well with experimental values[19] measured under white light (25 pm/V) and dark (6 pm/V), respectively. It is suggested that illumination could weaken the hydrogen bond between the MA cation and the inorganic Pb−I scaffold, thus effectively reducing the rotational barrier of the MA cation.[35] This allows the formation of a more polar structure with aligned MA cations in the presence of an electric field, which could arise from the photovoltage across the thin film. Therefore, the light-enhanced piezoelectric response is likely due to the transformation of a configuration with less-ordered molecular orientation (e.g., M2-like) to a configuration with more-ordered molecular orientation (e.g., M1-like).

To reveal the origin of piezoelectricity, we decompose the total polarization into the contributions from the *A*-site MA cations and *B*-site Pb atoms in M1. The polarization from Pb is estimated with $P_{Pb} = Z^*_{33}(Pb) \times D(Pb)/V_u$, where V_u is the volume of the primitive unit cell (1/4 of the volume of the tetragonal supercell), $Z^*_{33}(Pb)$ is the Born effective charge of Pb, and $D(Pb)$ is the average displacement of Pb along the *c* axis with respect to the center of its I_6 cage. The calculated value of $Z^*_{33}(Pb)$ is +4.24, significantly larger than the nominal charge of Pb (+2.0) in a pure ionic picture. This indicates the strong covalency of the Pb−I bonds and the presence of dynamic charge transfer coupled to the change of Pb−I bond length. The polarization from MA^+ molecules is approximated with $P_{MA} = \mu \cos(\theta)/V_u$, where μ is the dipole of the MA^+ molecule

DOI: 10.1021/acs.jpclett.6b00527
J. Phys. Chem. Lett. 2016, 7, 1460−1465

and θ is the average angle between the molecular dipole and the c axis. The site-resolved polarization and d_{33} are presented in Figure 3a. It is clear that although both Pb displacements and molecular dipoles are responsible for the total polarization, Pb atoms contribute nearly all of the piezoelectric response, with the contribution from the MA^+ molecules negligible. As shown in Figure 3b, the angle between the MA^+ and the c axis remains nearly constant, while the atomic displacement of Pb changes linearly with the stress.

We further explore the effect of chemical substitution on the piezoelectric properties of OMHPs. Table 2 presents the values

Table 2. Ground-State Polarization along the c axis (P_c) in $\mu C/cm^2$, Piezoelectric Coefficients d_{33} in pC/N, and e_{33} in C/m^2 for Various OMHPs of M1 and M2 Configurations

	M1			M2		
OMHP	P_c	d_{33}	e_{33}	P_c	d_{33}	e_{33}
$MAPbI_3$	5.59	31.4	0.83	0.07	3.1	0.07
$MASnI_3$	7.75	100.9	1.85	−0.22	23.7	0.51
$MAGeI_3$	13.68	27.4	0.49	8.92	32.4	0.52
$MAPbCl_3$	5.96	6.7	0.16	−0.01		
$MASnCl_3$	5.46	4.1	0.05	0.01		
$CF_3NH_3PbI_3$	15.8	248	1.59	−0.09	4.23	0.16

of d_{33} and e_{33} for $MAPbI_3$, $MASnI_3$, $MAGeI_3$, $CF_3NH_3PbI_3$, $MAPbCl_3$, and $MASnCl_3$. For all of the materials investigated, the M2 configuration has lower polarization and smaller d_{33} and e_{33} than the M1 configuration. It is noted, however, that $MAGeI_3$ of M2 configuration still has a moderate polarization of 8.92 $\mu C/cm^2$ despite the molecular dipoles nearly canceling each other out. Close examination of the structure reveals that the Ge atom is displaced by 0.23 Å away from the center of I_6 cage. The significant displacement is due to the small size of Ge relative to the large A cations and I_6 octahedron. As shown in Figure 4, for $MAPbI_3$, $MASnI_3$, and $MAGeI_3$, three OMHPs

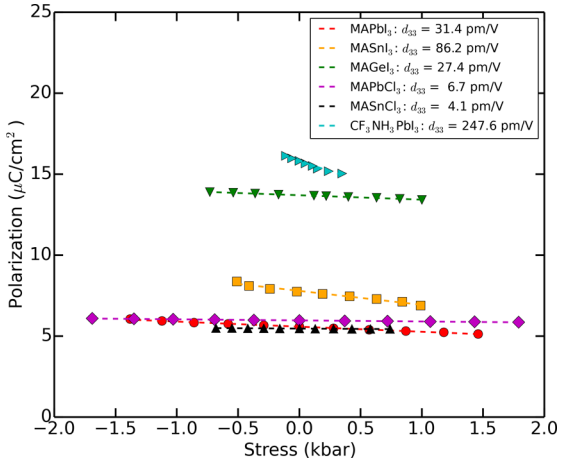

Figure 4. Stress dependence of polarization for various OMHPs, all with M1 molecular orientation.

differing only by the B-site element, $MAGeI_3$ M1 has the highest polarization, while $MASnI_3$ M1 has the highest piezoelectric coefficient (d_{33} = 100.9 pC/N), comparable to classic inorganic ferroelectric $PbTiO_3$ (d_{33} = 80 pC/N).[32] The higher d_{33} in $MASnI_3$ is attributed to the larger Born effective charge Z^*_{33}(Sn) = +4.64, compared with Z^*_{33}(Ge) = +3.60 and Z^*_{33}(Pb) = +4.24. Comparing $MAPbCl_3$ and $MASnCl_3$ to $MAPbI_3$ and $MASnI_3$, we find that substituting I with Cl dramatically reduces d_{33} and e_{33}, which can be explained by the reduced covalency (more ionic character) of Pb(Sn)−Cl bonds. Born effective charge calculations show that Z^*_{33} of Sn is reduced to +3.39 in $MASnCl_3$. This means a smaller charge transfer and thus less polarization change will occur upon change of the Sn−Cl bond length, causing smaller piezoelectric response.

As demonstrated with $CF_3NH_3PbI_3$, replacing the MA^+ with a more polar molecular cation greatly increases both the polarization and the piezoelectric response. The larger molecular dipoles not only contribute directly to the polarization but also increase the hydrogen-bonding strength between NH_3 and I, which indirectly weakens the bonding between I and Pb. This is supported by the larger Pb displacement (~0.30 Å) under zero stress condition compared with that of ~0.09 Å in $MAPbI_3$. In other words, the Pb atoms in $CF_3NH_3PbI_3$ have a softer potential energy surface and therefore a stronger response to external perturbation, resulting in higher piezoelectricity.

Many processes may contribute to the light-induced molecular dipole reorientation. Here we discuss possible mechanisms for the light-enhanced piezoelectricity in more detail. It is suggested that the light illumination, by weakening the hydrogen bond between the MA cation and the inorganic PbI_3 sublattice, could make the molecular cations easier to rotate and to align with external field. This is supported by DFT calculations, which reveal a reduced binding energy of the MA cation to the inorganic cage at the triplet state.[35] Additionally, as the band gap of $MAPbI_3$ is in the visible-light region, a significant amount of above-band-gap excitation occurs, with the excess energy dissipating as heat (kinetic energy of molecules) when the hot carriers relax to the band edges. We have recently shown that the molecules play an important role in carrier relaxation, with MA translation, CH/NH twisting, and CH/NH stretching modes assisting the process.[36] We thus develop a simple analytical model here to examine the magnitude of light-induced thermalization in a $MAPbI_3$ thin film.[37] Shown in Figure 5a is the absorption spectrum $\alpha(E)$ computed from the DFT optical dielectric function. The dielectric function is summed over the Brillouin zone and enough empty bands to converge. Assuming that all of the energy released from hot carrier relaxation is transformed into kinetic energy (κ) of molecules, the average thermal energy received by each molecule at depth D per second can be estimated as

$$\kappa(D) = A\int_{E_g}^{\infty} dE\, \frac{I_0(E)e^{-\alpha(E)D}(E - E_g)}{E}(1 - e^{-\alpha(E)\Delta d}) \quad (3)$$

where $I_0(E)$ is the sunlight intensity spectrum, Δd is the thickness of a single layer of molecules (equal to the lattice constant of $MAPbI_3$, 0.63 nm), A is the area per molecule, and E_g is the band gap of 1.65 eV calculated from DFT. As plotted in Figure 5b, the energy obtained by a single molecule per second has a strong dependence on the depth due to the exponential decay of the light intensity. In particular, the molecules near the top surface of the sample can obtain significant energy (much larger than room-temperature energy scale) to overcome the barrier and reorient their dipole directions under the applied voltage, which is likely to result in a more polar structure with large piezoelectricity, as measured

DOI: 10.1021/acs.jpclett.6b00527
J. Phys. Chem. Lett. 2016, 7, 1460−1465

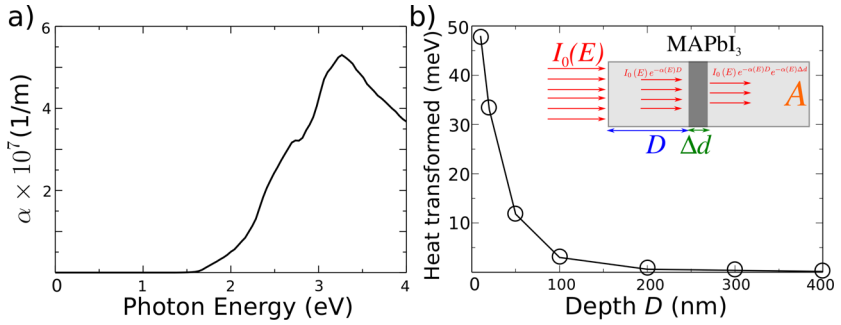

Figure 5. (a) DFT calculated absorption spectrum. (b) Estimation of the averaged energy transferred from the photoexcited carriers to each molecule at different depths (D) per second. The insert illustrates the model described by eq 3.

in the experiments. The reorientation of the molecular cations should occur rapidly (~picosecond time scale);[26,38] however, the adjustment of the inorganic Pb−I scaffold could be much slower.[39] Juarez-Perez et al. found that the low-frequency (<10^4 Hz) dielectric constant of $MAPbI_3$ is enhanced significantly upon light illumination,[40] which suggests a structural variation occurring on a time scale of 10^{-4} s. Recent experiments also find that the structural transformation in $MAPbI_3$ between the dark and the light is reversible.[39] It is also noted that as the lattice constants of $MAPbI_3$ change under temperature, the piezoelectric constants are expected to be strongly temperature-dependent. We also used the experimental absorption from ref 41 to compute the heat transfer, which shows very close value (11.2 meV) compared with DFT result (11.8 meV) for D = 50 nm. The DFT absorption spectrum overestimates the absorption in the high-energy range but slightly underestimates the low-energy range. The overall heat transfer to the molecule will not be significantly affected.

In summary, the piezoelectric properties of several OMHPs are studied with ab initio density functional theory. For $MAPbI_3$, the calculated piezoelectric coefficients of the polar and nonpolar configurations agree reasonably well with experimental values measured under white light and dark, respectively. This suggests a light-driven molecular reordering, which could be attributed to the weakened hydrogen bonds between MA cations and inorganic cages in the excited state and the thermalization arising from hot carrier relaxation. The photopiezoelectricity of OMHPs offers a potential avenue to optical transducers. Comparing the piezoelectric properties of OMHPs with different organic molecules, metal cations, and halide anions helps to identify several design principles for tuning the piezoelectric coefficients. We find that the atomic displacement of B-site metal cations is responsible for the piezoelectric response; therefore, creating a softer energy profile versus cation displacement is critical for enhancing d_{33} and e_{33}. Our finding highlights the potential of OMHPs for the design and optimization of functional photopiezoelectrics and photoferroelectrics.

AUTHOR INFORMATION

Corresponding Authors

*S.L.: E-mail: sliu@carnegiescience.edu.
*A.M.R.: E-mail: rappe@sas.upenn.edu.

Notes

The authors declare no competing financial interest.

ACKNOWLEDGMENTS

S.L. is supported by the Carnegie Insitution for Science and also acknowledges support from the National Science Foundation under grant CBET-1159736. F.Z. acknowledges the support of the Office of Naval Research, under grant N00014-14-1-0761. I.G. acknowledges the support of the Office of Naval Research, under grant N00014-12-1-1033. A.M.R. acknowledges the support of the Department of Energy Office of Basic Energy Sciences, under grant DE-FG02-07ER46431. All authors thank the National Energy Research Scientific Computing Center of the Department of Energy and the High-Performance Computing Modernization Office of the Department of Defense.

REFERENCES

(1) NREL. *Research Cell Efficiency Records*. http://www.nrel.gov/ncpv/images/efficiency_chart.jpg (accessed March 9, 2016).
(2) Kojima, A.; Teshima, K.; Shirai, Y.; Miyasaka, T. Organometal Halide Perovskites As Visible-Light Sensitizers for Photovoltaic Cells. *J. Am. Chem. Soc.* **2009**, *131*, 6050−6051.
(3) Baikie, T.; Fang, Y.; Kadro, J. M.; Schreyer, M.; Wei, F.; Mhaisalkar, S. G.; Graetzel, M.; White, T. J. Synthesis and Crystal Chemistry of the Hybrid Perovskite $(CH_3NH_3)PbI_3$ for Solid-State Sensitised Solar Cell Applications. *J. Mater. Chem. A* **2013**, *1*, 5628−5641.
(4) Im, J.-H.; Lee, C.-R.; Lee, J.-W.; Park, S.-W.; Park, N.-G. 6.5% Efficient Perovskite Quantum-Dot-Sensitized Solar Cell. *Nanoscale* **2011**, *3*, 4088−4093.
(5) Filip, M. R.; Eperon, G. E.; Snaith, H. J.; Giustino, F. Steric Engineering of Metal-Halide Perovskites with Tunable Optical Band Gaps. *Nat. Commun.* **2014**, *5*, 5757−1−9.
(6) Lee, M. M.; Teuscher, J.; Miyasaka, T.; Murakami, T. N.; Snaith, H. J. Efficient Hybrid Solar Cells Based on Meso-Superstructured Organometal Halide Perovskites. *Science* **2012**, *338*, 643−647.
(7) Etgar, L.; Gao, P.; Xue, Z.; Peng, Q.; Chandiran, A. K.; Liu, B.; Nazeeruddin, M. K.; Graetzel, M. Mesoscopic $CH_3NH_3PbI_3/TiO_2$ Heterojunction Solar Cells. *J. Am. Chem. Soc.* **2012**, *134*, 17396−17399.
(8) Stoumpos, C. C.; Malliakas, C. D.; Kanatzidis, M. G. Semiconducting Tin and Lead Iodide Perovskites with Organic Cations: Phase Transitions, High Mobilities, and Near-Infrared Photoluminescent Properties. *Inorg. Chem.* **2013**, *52*, 9019−9038.
(9) Zheng, F.; Saldana-Greco, D.; Liu, S.; Rappe, A. M. Material Innovation in Advancing Organometal Halide Perovskite Functionality. *J. Phys. Chem. Lett.* **2015**, *6*, 4862−4872.
(10) Jaffe, B.; Cook, W.; Jaffe, H. *Piezoelectric Ceramics*; Academic Press: New York, 1971.
(11) Ballato, A. Piezoelectricity: Old effect, New thrusts. *IEEE Transactions on Ultrasonics, Ferroelectrics and Frequency Control* **1995**, *42*, 916−926.

DOI: 10.1021/acs.jpclett.6b00527
J. Phys. Chem. Lett. 2016, 7, 1460−1465

(12) Frost, J. M.; Butler, K. T.; Brivio, F.; Hendon, C. H.; van Schilfgaarde, M.; Walsh, A. Atomistic Origins of High-Performance in Hybrid Halide Perovskite Solar Cells. *Nano Lett.* **2014**, *14*, 2584−2590.
(13) Liu, S.; Zheng, F.; Koocher, N. Z.; Takenaka, H.; Wang, F.; Rappe, A. M. Ferroelectric Domain Wall Induced Band Gap Reduction and Charge Separation in Organometal Halide Perovskites. *J. Phys. Chem. Lett.* **2015**, *6*, 693−699.
(14) Ma, J.; Wang, L.-W. Nanoscale Charge Localization Induced by Random Orientations of Organic Molecules in Hybrid Perovskite $CH_3NH_3PbI_3$. *Nano Lett.* **2015**, *15*, 248−253.
(15) Kutes, Y.; Ye, L.; Zhou, Y.; Pang, S.; Huey, B. D.; Padture, N. P. Direct Observation of Ferroelectric Domains in Solution-Processed $CH_3NH_3PbI_3$ Perovskite Thin Films. *J. Phys. Chem. Lett.* **2014**, *5*, 3335−3339.
(16) Xiao, Z.; Yuan, Y.; Shao, Y.; Wang, Q.; Dong, Q.; Bi, C.; Sharma, P.; Gruverman, A.; Huang, J. Giant Switchable Photovoltaic Effect in Organometal Trihalide Perovskite Devices. *Nat. Mater.* **2014**, *14*, 193−198.
(17) Fan, Z.; Xiao, J.; Sun, K.; Chen, L.; Hu, Y.; Ouyang, J.; Ong, K. P.; Zeng, K.; Wang, J. Ferroelectricity of $CH_3NH_3PbI_3$ Perovskite. *J. Phys. Chem. Lett.* **2015**, *6*, 1155−1161.
(18) Kim, H.-S.; Kim, S. K.; Kim, B. J.; Shin, K.-S.; Gupta, M. K.; Jung, H. S.; Kim, S.-W.; Park, N.-G. Ferroelectric Polarization in $CH_3NH_3PbI_3$ Perovskite. *J. Phys. Chem. Lett.* **2015**, *6*, 1729−1735.
(19) Coll, M.; Gomez, A.; Mas-Marza, E.; Almora, O.; Garcia-Belmonte, G.; Campoy-Quiles, M.; Bisquert, J. Polarization Switching and Light-Enhanced Piezoelectricity in Lead Halide Perovskites. *J. Phys. Chem. Lett.* **2015**, *6*, 1408−1413.
(20) Lefki, K.; Dormans, G. J. M. Measurement of Piezoelectric Coefficients of Ferroelectric Thin Films. *J. Appl. Phys.* **1994**, *76*, 1764.
(21) Perdew, J. P.; Burke, K.; Ernzerhof, M. Generalized Gradient Approximation Made Simple. *Phys. Rev. Lett.* **1996**, *77*, 3865−3868.
(22) Giannozzi, P.; Baroni, S.; Bonini, N.; Calandra, M.; Car, R.; Cavazzoni, C.; Ceresoli, D.; Chiarotti, G. L.; Cococcioni, M.; Dabo, I.; et al. Quantum ESPRESSO: A Modular and Open-Source Software Project for Quantum Simulations of Materials. *J. Phys.: Condens. Matter* **2009**, *21*, 395502−20.
(23) Rappe, A. M.; Rabe, K. M.; Kaxiras, E.; Joannopoulos, J. D. Optimized Pseudopotentials. *Phys. Rev. B: Condens. Matter Mater. Phys.* **1990**, *41*, 1227−1230.
(24) Ramer, N. J.; Rappe, A. M. Designed Nonlocal Pseudopotentials for Enhanced Transferability. *Phys. Rev. B: Condens. Matter Mater. Phys.* **1999**, *59*, 12471−12478.
(25) Zheng, F.; Takenaka, H.; Wang, F.; Koocher, N. Z.; Rappe, A. M. First-Principles Calculation of Bulk Photovoltaic Effect in $CH_3NH_3PbI_3$ and $CH_3NH_3PbI_{3-x}Cl_x$. *J. Phys. Chem. Lett.* **2015**, *6*, 31−37.
(26) Quarti, C.; Mosconi, E.; De Angelis, F. Structural and Electronic Properties of Organo-Halide Hybrid Perovskites from Ab Initio Molecular Dynamics. *Phys. Chem. Chem. Phys.* **2015**, *17*, 9394−9409.
(27) Sághi-Szabó, G.; Cohen, R. E.; Krakauer, H. First-Principles Study of Piezoelectricity in Tetragonal $PbTiO_3$ and $PbZr_{1/2}Ti_{1/2}O_3$. *Phys. Rev. B: Condens. Matter Mater. Phys.* **1999**, *59*, 12771−12776.
(28) Sághi-Szabó, G.; Cohen, R. E.; Krakauer, H. First-Principles Study of Piezoelectricity in $PbTiO_3$. *Phys. Rev. Lett.* **1998**, *80*, 4321.
(29) Bernardini, F.; Fiorentini, V. First-Principles Calculation of the Piezoelectric Tensor d of III−V Nitrides. *Appl. Phys. Lett.* **2002**, *80*, 4145.
(30) Bellaiche, L. Piezoelectricity of Ferroelectric Perovskites from First Principles. *Curr. Opin. Solid State Mater. Sci.* **2002**, *6*, 19−25.
(31) Nye, J. *Physical Properties of Crystals: Their Representation by Tensors and Matrices*; Oxford Science Publications, 1985.
(32) Shi, J.; Grinberg, I.; Wang, X.; Rappe, A. M. Atomic Sublattice Decomposition of Piezoelectric Response in Tetragonal $PbTiO_3$, $BaTiO_3$, and $KNbO_3$. *Phys. Rev. B: Condens. Matter Mater. Phys.* **2014**, *89*, 094105.
(33) Egger, D. A.; Kronik, L. Role of Dispersive Interactions in Determining Structural Properties of Organic−Inorganic Halide Perovskites: Insights from First-Principles Calculations. *J. Phys. Chem. Lett.* **2014**, *5*, 2728−2733.
(34) Grimme, S. Semiempirical GGA-type Density Functional Constructed With A Long-Range Dispersion Correction. *J. Comput. Chem.* **2006**, *27*, 1787−1799.
(35) Gottesman, R.; Haltzi, E.; Gouda, L.; Tirosh, S.; Bouhadana, Y.; Zaban, A.; Mosconi, E.; De Angelis, F. Extremely Slow Photoconductivity Response of $CH_3NH_3PbI_3$ Perovskites Suggesting Structural Changes Under Working Conditions. *J. Phys. Chem. Lett.* **2014**, *5*, 2662−2669.
(36) Zheng, F.; Tan, L. Z.; Liu, S.; Rappe, A. M. Rashba Spin−Orbit Coupling Enhanced Carrier Lifetime in $CH_3NH_3PbI_3$. *Nano Lett.* **2015**, *15*, 7794−7800.
(37) Li, L.; Wang, F.; Wu, X.; Yu, H.; Zhou, S.; Zhao, N. Carrier-Activated Polarization in Organometal Halide Perovskites. *J. Phys. Chem. C* **2016**, *120*, 2536−2541.
(38) Knop, O.; Wasylishen, R. E.; White, M. A.; Cameron, T. S.; Oort, M. J. M. V. Alkylammonium Lead Halides. Part 2. $CH_3NH_3PbX_3$ (X = Cl, Br, I) Perovskites: Cuboctahedral Halide Cages With Isotropic Cation Reorientation. *Can. J. Chem.* **1990**, *68*, 412−422.
(39) Gottesman, R.; Gouda, L.; Kalanoor, B. S.; Haltzi, E.; Tirosh, S.; Rosh-Hodesh, E.; Tischler, Y.; Zaban, A.; Quarti, C.; Mosconi, E.; et al. Photoinduced Reversible Structural Transformations in Free-Standing $CH_3NH_3PbI_3$ Perovskite Films. *J. Phys. Chem. Lett.* **2015**, *6*, 2332−2338.
(40) Juarez-Perez, E. J.; Sanchez, R. S.; Badia, L.; Garcia-Belmonte, G.; Kang, Y. S.; Mora-Sero, I.; Bisquert, J. Photoinduced Giant Dielectric Constant in Lead Halide Perovskite Solar Cells. *J. Phys. Chem. Lett.* **2014**, *5*, 2390−2394.
(41) Park, B.-W.; Jain, S. M.; Zhang, X.; Hagfeldt, A.; Boschloo, G.; Edvinsson, T. Resonance Raman and Excitation Energy Dependent Charge Transfer Mechanism in Halide-Substituted Hybrid Perovskite Solar Cells. *ACS Nano* **2015**, *9*, 2088−2101.
(42) Poglitsch, A.; Weber, D. Dynamic Disorder in Methylammoniumtrihalogenoplumbates (II) Observed by Millimeter-Wave Spectroscopy. *J. Chem. Phys.* **1987**, *87*, 6373−6378.

DOI: 10.1021/acs.jpclett.6b00527
J. Phys. Chem. Lett. 2016, 7, 1460−1465